Journal of Alloys and Compounds 479 (2009) 440–444

Contents lists available at ScienceDirect

Journal of Alloys and Compounds

journal homepage: www.elsevier.com/locate/jallcom

Influence of tungsten on the carbon nanotubes growth by CVD process

Mariano Escobar[a,b,*], Gerardo H. Rubiolo[b,d], M. Sergio Moreno[c], Silvia Goyanes[b], Roberto Candal[a]

[a] Instituto de Fisicoquímica de Materiales, Ambiente y Energía, CONICET-UBA, Pabellón II, Ciudad Universitaria (1428) Bs As, Argentina
[b] LP&MC, Dep. De Física, FCEyN-UBA, Pabellón 1, Ciudad Universitaria (1428) Bs As, Argentina
[c] Centro Atómico Bariloche, (8400) S.C. de Bariloche, Río Negro, Argentina
[d] Unidad de Actividad Materiales, CNEA, Av. Gral. Paz 1499, San Martin (1650), Bs As, Argentina

ARTICLE INFO

Article history:
Received 17 May 2008
Received in revised form 19 December 2008
Accepted 23 December 2008
Available online 4 January 2009

Keywords:
Carbon nanotubes
Tungsten
Chemical vapor deposition

ABSTRACT

The effect of tungsten (W) on the growth of multi-walled carbon nanotubes (MWNTs) using the chemical vapour deposition (CVD) process over a metal Fe–W catalyst incorporated into a silica matrix is reported. A W molar content in Fe/SiO_2 up to 10% was studied. The incorporation of only 2% of W substantially modifies the crystalline phases and the crystalline degree of the catalyst during the MWNTs synthesis. This fact seems to have a strong influence on the type and yield of the carbonaceous species obtained by the CVD of acetylene, at 600 °C and 180 Torr, over each catalyst. Tungsten interacts with iron within the matrix, diminishing the catalytic activity of the metal nanoparticles, and both, carbon nanotubes and carbon nanofibers, are obtained when tungsten is present. The results obtained support the hypothesis of a base growth model for carbon nanotubes indicating a strong interaction between silica matrix and Fe/W nanoparticles, independently of the content of W.

1. Introduction

Industrial applications of carbon nanotubes (CNTs) demand the development of synthetic processes, which are able to produce the material at low cost, with high purity and on large scale. Chemical vapor deposition (CVD) is considered to be one of the most promising routes to satisfy these requirements [1,2]. As a result, current research has focused on the optimization of the CVD process, i.e., by investigating the effect of catalyst composition, variation of supporting/substrate materials, synthesis temperature and hydrocarbon sources [3].

Multi-walled carbon nanotubes (MWNTs) can be grown on supported transition metals nanoparticles (Fe, Co, and Ni) or a combination of them. Several authors have suggested that iron (Fe) is the most active catalyst for the production of CNT [3], although several characteristics (such as wall multiplicity, length and synthesis yield) can be modified by the incorporation of other transition metals such as Co, Ni, Mo, Pd, amongst others [4–8]. One of the most explored mixed systems is Fe–Co, however, the results reported to date show some disparities. Cheng et al. [9] showed that Fe–Co supported on $CaCO_3$ is the most active catalyst and is quite promising for large-scale and low-cost production of CNTs compared to Fe, Ni, Co and their combinations. These results were in agreement with those reported by Somanathan et al. using mesoporous silica as a support [10]. On the other hand, Tran et al. [11] reported that the Fe–Co bimetallic catalyst was less efficient than a pure Co-based catalyst supported on alumina. These disparities suggest that the support plays an important role in the synthesis process [2]. In the case of the Fe–Mo catalytic system it seems to be less conflicting results, where several authors have shown that incorporation of Mo to Fe nanoparticles leads to the production of single and double wall CNT [12,13]. Similar behaviour was reported for Co–Mo systems [14,15].

The use of tungsten (W) as a catalyst for MWCNT growth was reported in very few papers [16,17]. In the reported syntheses a two-stage furnace was employed where W was deposited on the oven walls by thermal decomposition. To our knowledge, the use of silica supported Fe–W catalyst in CVD process for the production of carbon nanotubes has not yet been reported. This system presents an interesting case to study the existence of competitive or synergic effects between the two catalysts since the individual metals both have the capability to produce CNTs. Furthermore, the chemical similarities between Mo and W as well as the existence of carbon tungstates can play a role in the synthetic process.

Therefore, this paper reports the effect of tungsten on the synthesis of CNTs by the CVD process using a Fe–W metal catalyst supported on a SiO_2 matrix. A relationship between the crystalline

* Corresponding author at: Instituto de Fisicoquímica de Materiales, Ambiente y Energía, Ciudad Universitaria, Pabellón II (1428) Buenos Aires, Argentina.
Tel.: +54 11 4576 3380x113; fax: +54 11 4576 3341.
E-mail address: mescobar@qi.fcen.uba.ar (M. Escobar).

0925-8388/$ – see front matter © 2009 Elsevier B.V. All rights reserved.
doi:10.1016/j.jallcom.2008.12.104

phases present in the catalyst and the growing rate of carbon nanotubes was observed.

2. Experimental

Mesoporous silica containing doped-iron nanoparticles was prepared by the sol–gel process reported by Pan et al. [18]. The molar content of W studied in the Fe/SiO_2 system was 0, 2, 5 and 10%mol/mol (with respect to the iron content). In a typical synthesis, 7.5 ml of iron nitrate (Riedel de Hagen) aqueous solution (1.5 M) was mixed with tungsten ethoxide (5%V in ethanol Alfa Aesar) (in stoichiometric quantities) and ethanol under magnetic stirring. Subsequently, 5 ml of tetraethyl orthosilicate (Aldrich) was added as the silica precursor. After 20 min of magnetic stirring, a few drops of concentrated hydrogen fluoride (0.4 ml) (Merck) was then added and stirred for another 20 min. In all cases the total amount of ethanol used was 10 ml. The mixture was then dropped onto a quartz plate to form a film with a thickness of 3–5 mm. After gelation of the mixture, the gel was dried overnight at 80 °C to remove excess water and ethanol. During this step the gel cracked into small pieces of xerogel with areas between 5 and 20 mm^2. The substrates were then placed in a quartz boat and were subsequently introduced into the chamber of a tube furnace, where a three-step thermal treatment was applied. Initially, the substrates were fired at 450 °C for 10 h in air. Secondly, the temperature was rised to 600 °C and the substrates were reduced during 4 h in a flow of 9% hydrogen in nitrogen with an overpressure of 180 Torr. The third and final step involved the introduction of 3 sccm of acetylene diluted in 107 sccm of nitrogen (2.5% of acetylene in nitrogen) were introduced into the chamber. During this final step, the carbon nanotubes were formed on the substrates by deposition of carbon atoms from decomposition of acetylene at 600 °C under 180 Torr. The growth time was 3 h. After the growth of carbon nanotube, the furnace was cooled to the room temperature under nitrogen gas flow.

X-ray diffraction patterns (XRDs) were recorded for different stages of the substrate synthesis using a Siemens D5000 X-Ray diffractometer, with Cu Kα radiation and a graphite monochromator. High Resolution Transmission Electron Microscopy (HR-TEM Philips CM200) and Field Emission Scanning Electron Microscopy (FEG-SEM Zeiss LEO 982 GEMINI) were employed to study the different morphologies. Thermogravimetric Analysis (Shimadzu TGA-51) and Differential Thermal Analysis (Shimadzu DTA-50) were performed on 15 mg samples with a heating rate of 10 K/min and airflow of 50 cm^3/min. When necessary, the nanotubes samples were detached from the catalyst by ultrasonic dispersal in ethanol.

3. Results and discussion

3.1. Effect of W on the Fe/SiO_2 phases

Fig. 1 shows the XRD patterns of the catalysts fired at 450 °C for 10 h in air. Fig. 1a corresponds to the Fe/SiO_2 system and shows a typical γ-Fe_2O_3 pattern indicating that the iron oxide nanoparticles were in fact crystalline. The peaks are wide and poorly defined as a consequence of the small crystallite size (4.8 nm as calculated from Scherrer equation). These observations are in agreement with previous works reported by Del Monte et al. in similar systems [19].

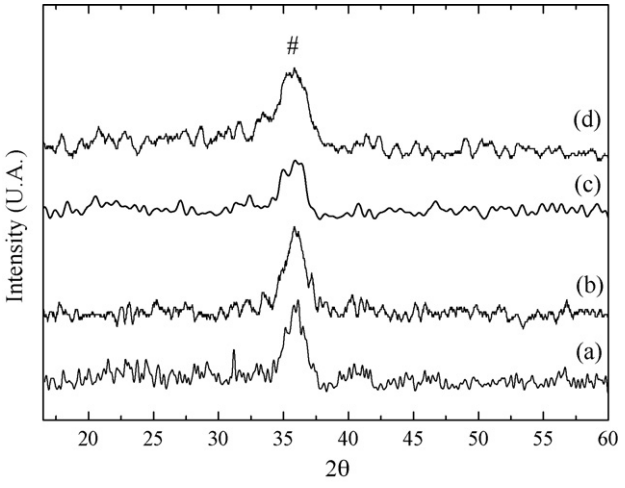

Fig. 1. XRD patterns of W–Fe/SiO_2 composites for 0, 2, 5 and 10%mol/mol (with respect to the iron content) W (curves a, b, c and d, respectively) fired at 450 °C in air. # corresponds to γ-Fe_2O_3.

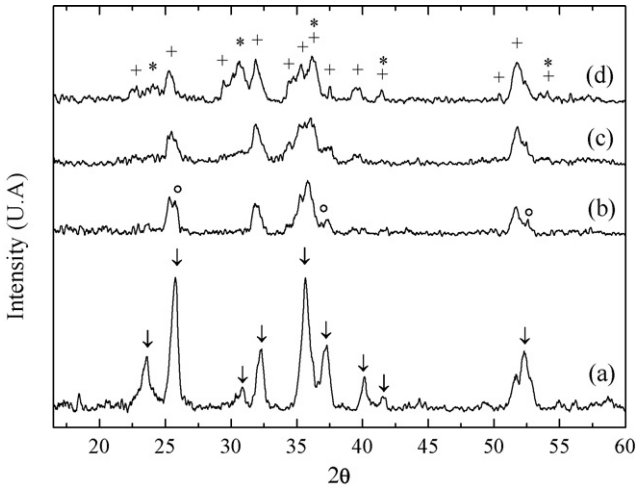

Fig. 2. XRD patterns of W–Fe/SiO_2 composites for 0, 2, 5 and 10%mol/mol W (curves a, b, c and d, respectively) after reduction at 600 °C for 4 h in a flow of 9% hydrogen in nitrogen; '↓' corresponds to laihunite phase, '+' corresponds to fayalite phase, '*' corresponds to ferberite phase ($FeWO_4$) and '◦' corresponds to tungsten oxide (WO_2).

However, it should be noted that minor changes in the synthesis can lead to different behaviors. For example, using a similar synthesis procedure, Perez-Cabero et al. observed a hematite crystalline phase in the xerogel fired at 450 °C where the main difference in the synthesis procedure was the presence of HCl acid as a catalyst [20].

The XRD also showed that as the concentration of tungsten was increased, the peak centered at $2\theta = 36°$ was broadened indicating a decrease in the crystallinity of the sample. It was also observed that in the 10%W sample this peak was broadest and also possessed a small shoulder at $2\theta = 33.5°$, perhaps indicating that a new crystalline phase associated with tungsten appears at high W(VI) concentration.

Fig. 2 shows the XRD pattern of the reduced catalyst. Laihunite ($Fe_{1.6}SiO_4$) is the predominant phase in the Fe/SiO_2 composite (Fig. 2a). When tungsten is incorporated into the composite, important changes in the crystalline phases and domain size are observed. As the concentration of tungsten increases, fayalite (Fe_2SiO_4) becomes the predominant phase to the detriment of the laihunite phase. Furthermore, a considerable reduction in the crystalline domains was also observed (see Fig. 2b and c). Other W-rich phases were also observed with increasing tungsten concentration. In samples containing 2 or 5% of tungsten, peaks corresponding to WO_2 can be observed at $2\theta = 25.7°$ (see Fig. 2b and c). Moreover, with 10% tungsten concentration, ferberite ($FeWO_4$), a new phase rich in tungsten was detected (Fig. 2d). These results were indicative of the fact that the reduction treatment was insufficient in reducing all the W(VI) to W(IV) for high W concentration.

It is interesting to note that a mere concentration of 2% of tungsten is sufficient to change the predominant crystalline phases and to reduce the crystallinity of the system. The dominance of the fayalite phase over the lahiunite phase when tungsten is present in the catalyst may be related to the lower degree of crystallinity of these systems. The smaller crystalline domain may improve the efficiency of the reduction process leading to the production of the more reduced phase: fayalite.

These results suggest that tungsten and iron are jointly distributed into the SiO_2 matrix, and as a result, both species can interact with each other. Thus, the presence of tungsten decreases the crystallinity of the iron-containing phases and modifies the phase changes that occur upon reduction with H_2/N_2. The strong interaction between iron and tungsten oxides can be explained by the fact that Fe(III) hydrolyzes at a high rate when it is dissolved in water, producing nuclei of iron oxide hydroxide precursors (typi-

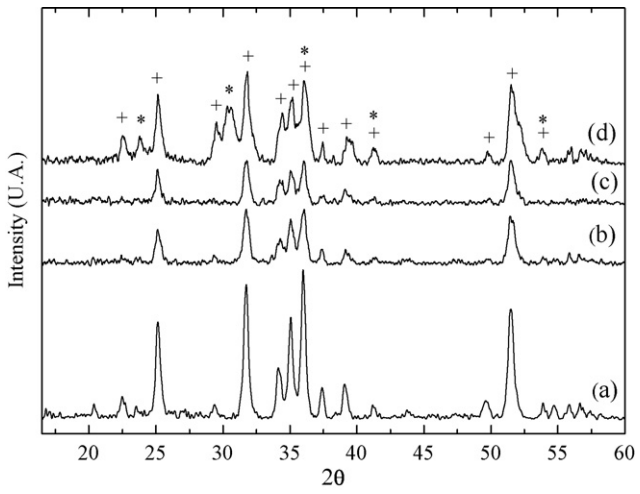

Fig. 3. XRD patterns of W–Fe/SiO_2 composites for 0, 2, 5 and 10%mol/mol W (curves a, b, c and d, respectively) after decomposition of acetylene at 600 °C for 3 h. '+' corresponds to fayalite phase (Fe_2SiO_4) and '*' corresponds to ferberite phase ($FeWO_4$).

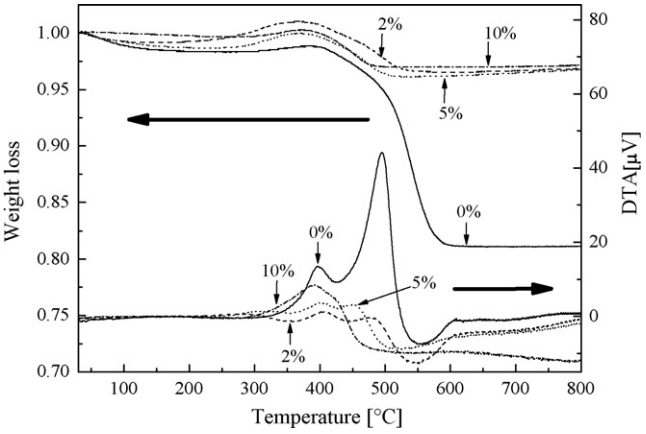

Fig. 4. TGA and DTA of samples obtained after deposition of carbon on all catalysts system in air.

cally iron oxohydroxides) [21]. These small nuclei must be positively charged under the acidic reaction media, because the isoelectric point of iron(III) oxohydroxides is close to 6.7 [22]. Based on the lower partial charge of W(VI) in $W(OEt)_6$ with respect to the partial charge of iron in $[Fe(H_2O)_6]^{3+}$ (0.43 and 0.59, respectively, see [21]), it is expected that the hydrolysis of the tungsten ethoxide precursor occurs at lower rate than the hydrolysis of Fe(III). The hydrolysis of W (VI) under moderately acidic conditions produce negatively charged polytungstates [23], which may be adsorbed on the surface of the growing iron oxide nanoparticles, leading to a strong interaction between the iron and the tungsten oxides.

It should also be emphasized that XRD patterns corresponding to metallic Fe or iron oxide phases were not detected after reduction treatment. This could perhaps be due to the fact that a small amount of particles is present, or that their particle sizes are near or below the detection limit of the XRD instrumentation.

Fig. 3 shows XRD patterns of the system formed by the composites and the carbonaceous structures obtained following treatment with a gaseous 2.5% acetylene–nitrogen mixture at 600 °C. In the case of the composites without tungsten (see Fig. 3a), the main crystalline phase, laihunite, is transformed to fayalite during the CNT synthesis. This transformation involves the reduction of all the Fe(III) present in laihunite to Fe(II), via reaction with the N_2–acetylene mixture and is also accompanied by a change in the crystalline structure. The presence of fayalite after CNT growth was previously reported [20,24]. The systems that contain tungsten as a component already have fayalite as main crystalline phase. However, the reductive thermal treatment improves the crystallinity without changing the crystalline phase (see Fig. 3b–d). In the case of 10% tungsten concentration, ferberite ($FeWO_4$) was also observed (Fig. 3d).

3.2. Effect of W on CNT and carbonaceous species

Fig. 4 shows the result of the TGA and DTA analysis of samples obtained from catalyst nanoparticles with different compositions. In the case of the pure iron nanoparticle catalyst, an increment of mass at ca. 350 °C was observed, which can be associated with the partial oxidation of the carbonaceous materials and/or the iron–silicon matrix. As the temperature increases there is an important loss of mass that can be assigned to two overimposed processes, corresponding to the oxidation of amorphous carbon and CNT, as will be discussed later. When W is incorporated into the catalyst, the increment of mass observed in the range 270–380 °C was slightly higher than in the previous case. This effect may be a consequence of the presence of WO_2, in particular in the samples with 2 and 5% concentration of W (as shown in Fig. 2b and c). The TGA plots clearly show that the carbon yield decrease with the amount of tungsten incorporated in the catalyst. Only 2% tungsten was enough to decrease the carbon yield by approximately 98%. DTA analysis of the samples obtained from pure iron nanoparticles show a small peak centered at 396 °C followed by a bigger peak centered at 494 °C. The first feature is assigned to amorphous carbon while the second is assigned to CNTs [24,25]. As the tungsten content in the catalyst nanoparticles was increased, the intensity of both peaks decreased as a consequence of the diminution of the carbon yield. However, the relative intensity of the amorphous carbon peak with respect to the CNTs peak was increased. In the case of 10%W, the CNT feature disappeared completely. These results

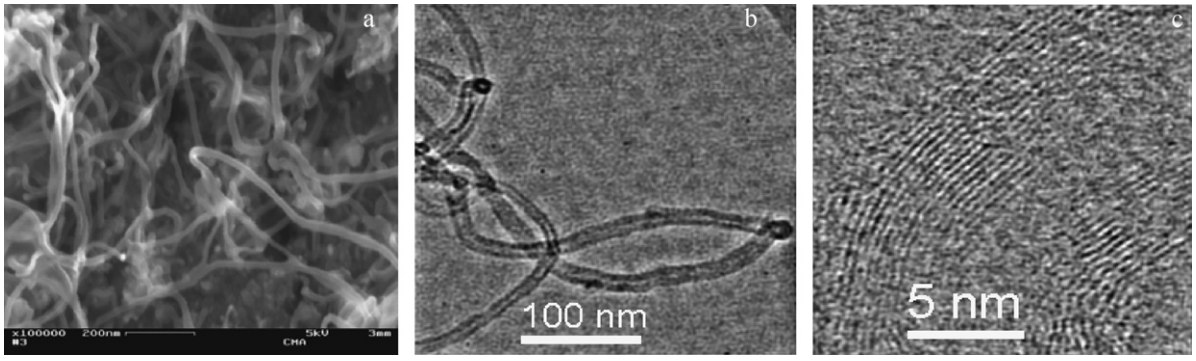

Fig. 5. FE-SEM, TEM and HRTEM images of carbon nanotubes obtained with Fe/SiO_2 catalyst.

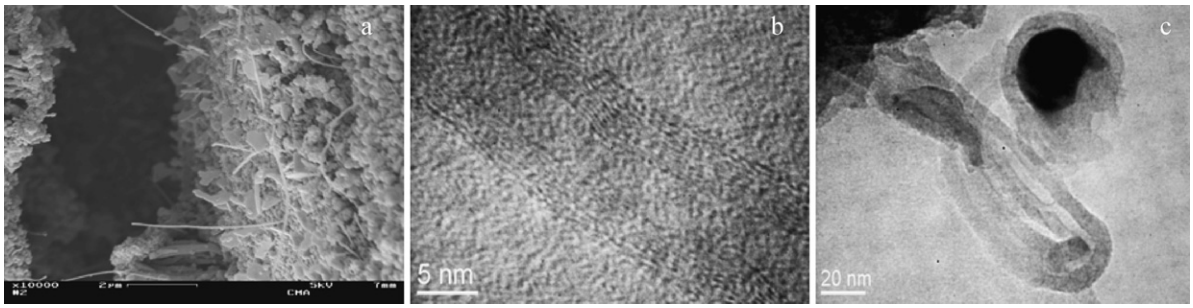

Fig. 6. SEM and TEM images of MWCNTs obtained with catalyst containing 2%mol/mol of W.

indicated that an increase in W in fact decreases the carbon yield and, in particular, the CNTs yield.

Fig. 5 shows SEM and HRTEM images of CNT grown on pure iron catalysts. The average outer diameter was observed to be 20 nm (Fig. 5a). Fig. 5b and c revealed the tubular structure of the nanotubes with an inner channel of ca. 4 nm. The CNTs are of the multi-wall kind, with a 3.22 Å separation between layers. Furthermore, on the right side of the micrograph in Fig. 5b, two nanotubes were observed to grow from the same particle, being the size of that nanoparticle bigger than the MWNT inner channel.

Fig. 6 shows the SEM and TEM micrographs of the carbonaceous material grown on iron catalysts containing 2% tungsten. Carbon fibers and MWNT were obtained with a low yield (Fig. 6a). In the case of the catalysts with 5 and 10% tungsten concentration the amount of carbonaceous materials was similar to 2%W, but MWNT were not detected. These results agree with the TGA and DTA analysis (see Fig. 4).

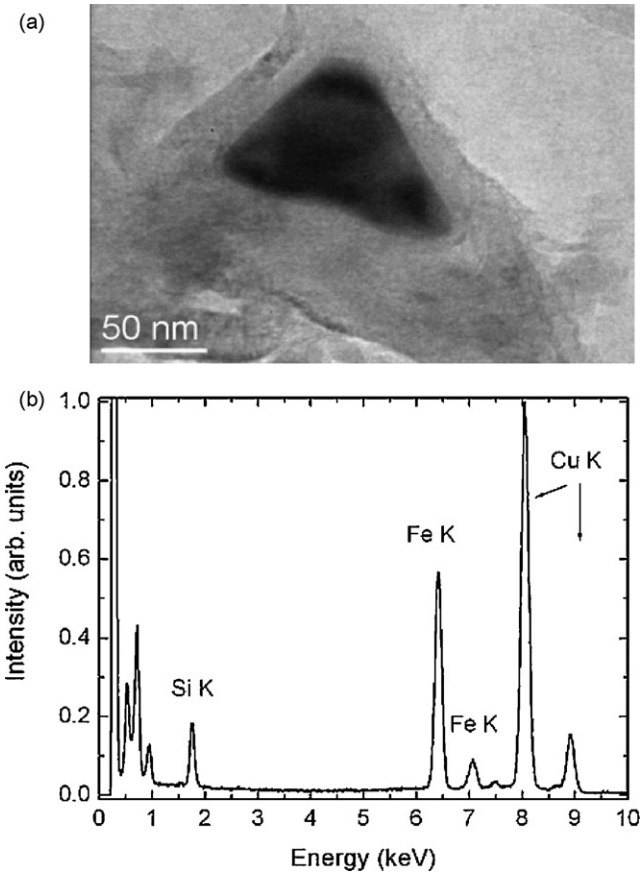

Fig. 7. TEM image and EDX spectrum of Fe/SiO_2 matrix containing 2%mol/mol of W.

It is interesting to note that Fig. 6c shows a MWNT tip surrounding a catalyst nanoparticle whose diameter is bigger than MWNT inner channel, as in the previous case (Fig. 5b). These images suggest that the synthesis of MWNT occurs through a base-growth mechanism [26]. It was proposed that the interactions between the catalyst particle and the support have a determinant role in the growth mechanism [3]. Weak interactions yield tip-growth mode whereas strong interactions lead to base-growth. In our case the interactions between the nanoparticles and the support are strong, due to the chemical affinity between the iron oxide nanoparticle precursor and the SiO_2 matrix. This hypothesis is supported by the TEM and EDX analyses performed on the silica matrix containing the metallic nanoparticles.

Fig. 7 shows a TEM image and EDX spectrum of a small area of the Fe/SiO_2 matrix containing 2% W. The dark spot observed in the figure is constituted by iron-rich nanoparticles as shown in the EDX analysis. The EDX spectrum of the nanoparticles shows a high content of Fe and a lower content of Si, indicating that iron nanoparticles are not completely isolated from the SiO_2 matrix, but included into the matrix. As discussed above, these results support the hypothesis of a base growth model in all the studied cases, independently of the content of tungsten.

4. Conclusion

The synthesis of the CNT occurs through a base-growth mechanism irrespective of the presence of tungsten on the catalyst system. This mechanism is the consequence of the strong interaction between metallic nanoparticles and the silica matrix. The incorporation of 2% of tungsten to the Fe/SiO_2 matrixes leads to two different effects. On the one hand there is a change in the crystalline phases in the reduced stage that predominates through the synthesis: maghemite → laihunite → fayalite, without tungsten; and maghemite → fayalite → fayalite, with 2% tungsten. On the other hand, the presence of tungsten inhibits the catalytic activity of the metal nanoparticles decreasing the yield of carbonaceous materials (amorphous, fibers and CNTs). These results suggest that when fayalite is the predominant crystalline phase during the nanoparticles reduction step, the catalytic activity of the metallic nanoparticles is notoriously decreased.

Acknowledgements

This work was supported by Universidad de Buenos Aires, Argentina (Investigation Project, X191); Consejo Nacional de Investigaciones Científicas y Técnicas (PIP 5215; PIP 5959) and Agencia Nacional de Promoción Científica y Tecnológica (PICT 10-25834; PICT 06-10621).

References

[1] A. Morancais, B. Caussat, Y. Kihn, P. Kalck, D. Plee, P. Gaillard, D. Bernard, P. Serp, Carbon 45 (2007) 624.

[2] G. Messina, V. Modafferi, S. Santangelo, P. Tripodi, M.G. Donato, M. Lanza, S. Galvagno, C. Milone, E. Piperopoulos, A. Pistone, Diamond Relat. Mater. 17 (2008) 1482.
[3] A. Dupuis, Prog. Mater. Sci. 50 (2005) 929.
[4] A. Policicchio, T. Caruso, G. Chiarello, E. Colavita, V. Formoso, R. Agostino, T. Tsoufis, D. Gournis, S. La Rosa, Surf. Sci. 601 (2007) 2823.
[5] S. Pirard, S. Douven, C. Bossuot, G. Heyen, J. Pirard, Carbon 45 (2007) 1167.
[6] B. Singh, S. Cho, K. Bartwal, N. Hoa, H. Ryu, Solid State Commun. 144 (2007) 498.
[7] Z. Balogh, G. Halasi, B. Korbély, K. Hernadi, Appl. Catal. A: Gen. 344 (2008) 191.
[8] T. Tsoufis, P. Xidas, L. Jankovic, D. Gournis, A. Saranti, T. Bakas, M. Karakassides, Diamond Relat. Mater. 16 (2007) 155.
[9] J. Cheng, X. Zhang, Z. Luo, F. Liu, Y. Ye, W. Yin, W. Liu, Y. Han, Mater. Chem. Phys. 95 (2006) 5.
[10] T. Somanathan, A. Pandurangan, Appl. Surf. Sci. 254 (2008) 5643.
[11] K. Tran, B. Heinrichs, J. Colomer, J. Pirard, S. Lambert, Appl. Catal. A 318 (2007) 63.
[12] R. Engel-Herbert, H. Pforte, T. Hesjedal, Mater. Lett. 61 (2007) 2589.
[13] S. Kang, K. Cho, K. Kim, G. Cho, J. Alloy Compd. 449 (2008) 269–273.
[14] S. Chai, S. Zein, A. Mohamed, Appl. Catal. A 326 (2007) 173.
[15] L. Zhang, Y. Tan, D. Resasco, Chem. Phys. Lett. 422 (2006) 198.
[16] Y. Huh, M. Green, J. Lee, C. Lee, Diamond Relat. Mater. 15 (2006) 100.
[17] C. Lee, S. Lyu, H. Kim, J. Park, H. Jung, J. Park, Chem. Phys. Lett. 361 (2002) 469.
[18] Z.W. Pan, S.S. Xie, B.H. Chang, L.F. Sun, W.Y. Zhou, G. Wang, Chem. Phys. Lett. 299 (1999) 97.
[19] F. Del Monte, M. Morales, D. Levy, A. Fernandez, M. Ocan, A. Roig, E. Molins, C. Serna, Langmuir 13 (1997) 3627.
[20] M. Perez-Cabero, I. Rodriguez-Ramos, A. Guerrero-Ruiz, J. Catal. 215 (2003) 305.
[21] J. Livage, M. Henry, C. Sanchez, Prog. Solid State Chem. 18 (1988) 259.
[22] G. Parks, Chem. Rev. 65 (1965) 177.
[23] C.F. Baes, R.E. Mesmer, The Hydrolysis of Cations, J. Wiley & Sons, NY, 1976.
[24] M.M. Escobar, S. Moreno, R.J. Candal, M.C. Marchi, A. Caso, P. Polosecki, G. Rubiolo, S. Goyanes, Appl. Surf. Sci. 354 (2007) 251.
[25] B. Ramesh, W. Blau, P. Tyagi, D. Misra, N. Ali, J. Gracio, G. Cabral, E. Titus, Thin Film Solid 494 (2006) 128.
[26] C. He, N. Zhao, C. Shi, X. Du, J. Li, J. Alloy Compd. 433 (2007) 79.